



Manufacture of Thin-Walled Axisymmetric Components by Friction Stir Welding and Spinning of Al-Li Alloy

HONGRUI ZHANG,^{1,2} MEI ZHAN^{1,4} ,^{1,4} ZEBANG ZHENG,^{1,2,5}
RUI LI,¹ WEI LYU,¹ XIAOLEI CUI,¹ SHUWAN CHEN,¹
and SHIJUN SHEN³

1.—Shaanxi Key Laboratory of High Performance Precision Forming Technology and Equipment, School of Materials Science and Engineering, Northwestern Polytechnical University, Xi'an 710072, China. 2.—Key Laboratory of High Performance Manufacturing for Aero Engine (Ministry of Industry and Information Technology), School of Mechanical Engineering, Northwestern Polytechnical University, Xi'an 710072, China. 3.—Shanghai Aerospace Equipment Manufacturer, China Aerospace Science and Technology Corporation, Shanghai 200245, China. 4.—e-mail: zhanmei@nwpu.edu.cn. 5.—e-mail: zebang.zheng@nwpu.edu.cn

A novel hybrid manufacturing technique combining friction stir welding and spinning provides a promising approach to forming large-diameter thin-walled axisymmetric components while minimizing process scrap. By integrating experimental and numerical methods, the feasibility of the hybrid manufacturing technique for producing thin-walled axisymmetric components with the 2195 Al-Li alloy was explored. The results indicate that the welding seam of the spun components restricts plastic deformation, which leads to flange swing. The movement of the welding seam occurs during spinning, and the movement direction is consistent with the rotation direction of the spun components. The microhardness of the components in the welding zone was found to increase by 21% on average after spinning. Moreover, the yield strength in the welding zone increased by over 60% and the tensile strength by over 12%. These results suggest that the hybrid manufacturing technique is a feasible way to produce large-diameter thin-walled axisymmetric components. Since the process scraps can be re-utilized using this method, it thus provides a potential route for sustainability in the recycling and remanufacturing of aluminum alloys.

INTRODUCTION

With the development of new sophisticated equipment, components with large load-carrying capacity, long service life, low energy consumption, and sustainable processes have gradually become the mainstream tendency in industrial fields. However, the material and structure of components play an essential role in meeting the above requirements. Therefore, lightweight high-strength materials and thin-walled curved surface structures, with the advantages of high performance, high reliability, and low cost have been widely employed as key

components in various industries, including aviation, aerospace, weapon, automobile, energy, electronics, and medical industries.¹⁻⁵ Some representative examples are components for spacecraft bulkheads, aircraft engines, radar reflectors, DNA separator enclosures, cymbals, and domestic utensils. Naturally, as a lightweight high-strength material, the 2195 Al-Li alloy has been successfully applied in thin-walled curved surface components (TWCSs) of the aerospace industry in recent years.^{6,7}

In addition, with the rapid development of large carrying equipment, manufacturing large-diameter TWCSs have been an urgent need. Currently, these large-diameter TWCSs are usually manufactured by two methods: one the conventional combination manufacturing process of stamping

(Received January 17, 2022; accepted June 23, 2022;
published online July 25, 2022)

and tailor welding (Fig. 1a), and the other by spin forming (Fig. 1c). However, compared with spin forming (Fig. 1c). However, compared with spin forming, the conventional combination manufacturing process has many disadvantages, with multi-piece, welded construction of TWCSCs with complex process equipment and manufacturing processes leading to high cost, inefficient manufacturing practices, high failure risk, low shape precision, and large residual stress. Consequently, spin forming is usually one of the major preferred approaches to manufacturing TWCSCs, due to many inherent advantages and flexible processes, such as simple tooling, low forming loads, and high material utilization.⁸⁻¹⁰

However, up to now, it has proved difficult to produce ultra-wide blanks with a size beyond 5 m, due to the limitations of the manufacturing

equipment load and process technology. Consequently, available technologies are insufficient to manufacture high-quality single-piece wide blanks for the spin forming of large-diameter TWCSCs from single integrated blanks (SIBs), which largely limits the development and application of such components. Recently, with the development and maturity of friction stir welding (FSW) technology of aluminum alloys, joint reliability and welding properties have been significantly and effectively improved. Thereby, a hybrid manufacturing technology that combines spinning and FSW provides a feasible manufacturing route for forming large-diameter TWCSCs. Meanwhile, the manufacturing technique can to some extent overcome the above-mentioned negative problems of the conventional combination manufacturing process of stamping

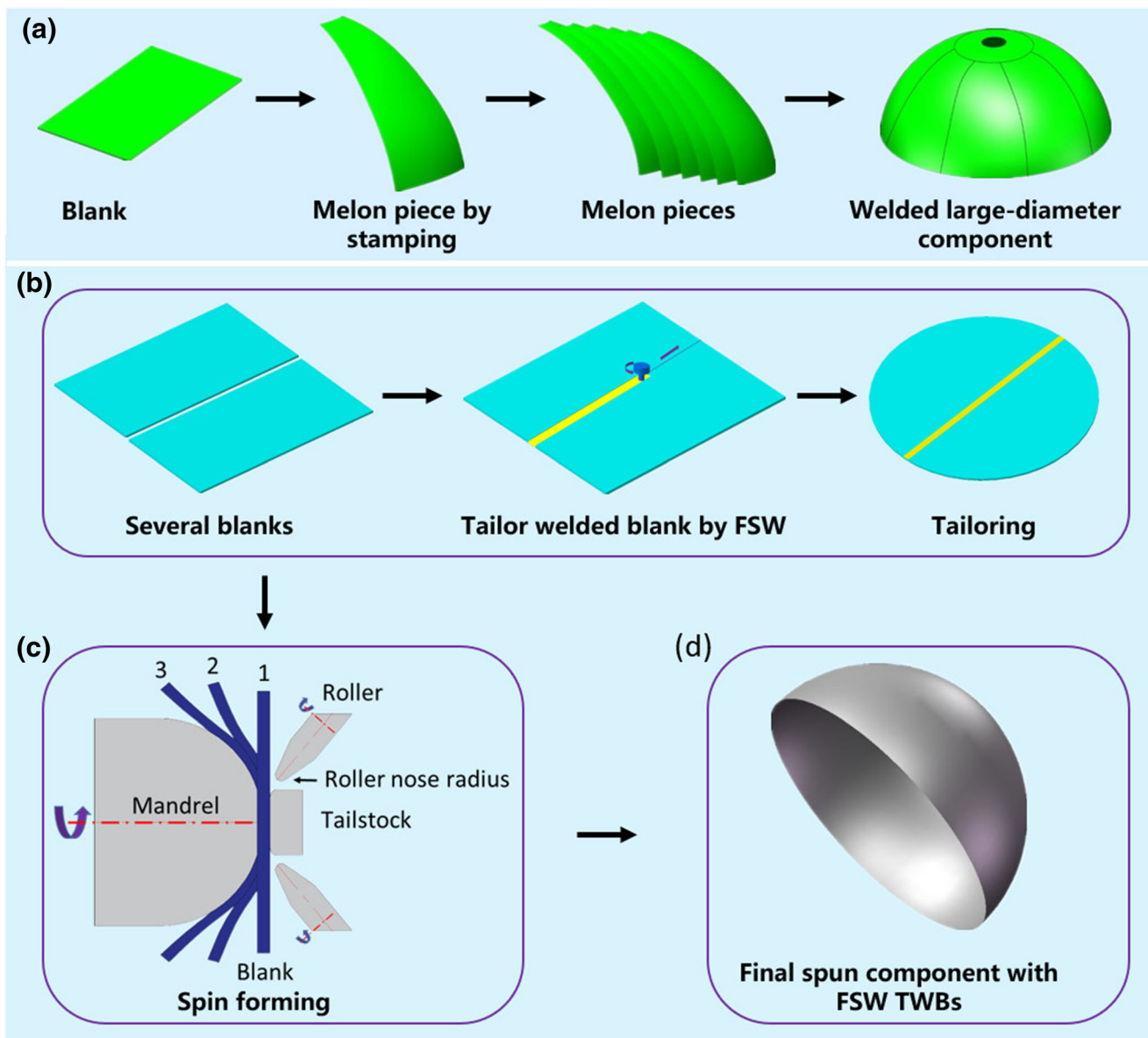


Fig. 1. Manufacturing methods for large-diameter thin-walled curved surface components: (a) conventional combination manufacturing process and (b-d) spinning process with tailor-welded blanks.

and tailor welding. In addition, aluminum alloy process scraps in industries can also be recycled and tailor-welded into the raw blanks for the spin forming of TWCSs, which will become a promising sustainable manufacturing method. In this study, to explore the process feasibility of the hybrid manufacturing method, spinning experiments for TWCSs were carried out based on small-size FSW tailor-welded blanks (TWBs). The hybrid manufacturing technique based on FSW and TWBs spinning is clearly shown in Fig. 1b–d. While the manufacturing of spin-formed TWCSs with TWBs is an extremely complex process, in which the material undergoes a large amount of local inhomogeneous deformation. In addition, the material properties of TWBs in the welding zone (WZ) have a significant difference from the base material zone (BMZ), which results in different deformation behaviors between the WZ and the BMZ, and deeply intensifies the inhomogeneous deformation in spinning.¹¹ Thus, it is important to investigate the process feasibility for spinning TWCSs with FSW TWBs.

In order to manufacture lightweight thin-walled components with TWBs, a multitude of studies on the formability of TWBs have been carried out, and some significant breakthroughs under different manufacturing processes have been made. Merklein et al.¹² mentioned that TWBs are suitable for lightweight designs for components with no reinforcing blanks and fewer joining elements. Liu et al.¹³ employed hot stamping tests on AA6082 TWBs to investigate the deformation behaviors and failure features, and forming-limit prediction models were developed and further integrated into finite element (FE) simulation based on a cloud-based multi-objective platform to investigate the failure/necking features of AA6082 TWBs. Abbasi et al.¹⁴ developed a new analytical method for the prediction of the weld line movement and dome height of TWBs during stretch forming. The results of FE simulations and experiments are in good agreement with the analytical results, which indicate that the analytical method is reliable. Ma et al.¹⁵ built a theoretical calculation model for the forming-limit diagram of TWBs based on plastic constitutive relationships and Hosford yield criteria. In addition, Parente et al.¹⁶ carried out a series of experiments to investigate the formability performance of TWBs produced by FSW with dissimilar aluminum alloy thin sheets, and the results showed that TWB formability depended on weld line orientation. With the assistance of FE simulation, Wang et al.¹⁷ investigated the movement laws of weld seams and factors affecting the formability of TWBs square cups with different strength combinations and different thickness combinations. Zhang et al.¹⁸ studied the influence laws of non-linear weld seam locations on the weld seam movement of TWBs with FE simulation and a rectangular box-stamping

experiment. Through FE simulation, Yin et al.¹⁹ simulated the stamping forming process of the middle channel of automobile panels produced by TWBs with different thicknesses. Thus, the spring-back process of TWBs was analyzed during the forming process. Simultaneously, Ma et al.²⁰ established a multipoint incremental forming FE simulation model to discuss the feasibility of the sphere and pyramid components forming with TWBs, by employing an explicit FE analysis software. In addition, many meaningful achievements on TWBs were successfully acquired in the cup-stamping process,²¹ the square box-stamping process,²² the V-bending process,²³ the U-bending process,²⁴ and the square box hydro-forming process²⁵ with FE simulations.

As a consequence, the achievements involved in TWBs have been attained by a multitude of researchers, which have significantly contributed to the development and application of TWBs in various industries. However, the previous efforts have been more concentrated on simple forming processes, such as stamping, bending, hydro-forming, and so on. Up to now, only a little research on TWBs spin forming has been carried out, e.g., by Zhang et al.^{26,27} Therefore, there is an urgent need to explore the process feasibility for spin-forming TWCSs with 2195 Al-Li alloy TWBs.

In this study, the feasibility of a novel hybrid manufacturing technique that combines FSW and spinning for forming TWCSs is investigated via FE simulations and experiments. It has been found that, during spinning, the welding seam restricts the material flow and plastic deformation, which leads to flange swing. Meanwhile, the deflection of the welding seam occurs after spinning. TWCSs were obtained using the hybrid manufacturing method. The microstructure, hardness, and mechanical properties of the spun components were significantly improved after spinning. The feasibility of the hybrid manufacturing technique was validated by this study, and provides a solution for addressing the forming of large-diameter TWCSs in industries, and adds a potential approach for recycling and reusing of aluminum alloy process scraps.

THE HYBRID MANUFACTURING TECHNIQUE BASED ON FSW AND SPINNING

The TWB spin-forming process for the TWCSs is an innovative hybrid manufacturing technique that combines FSW and spinning. Figure 1b–d shows the whole procedure of the TWB spin-forming process. First, several blanks are welded together by FSW. Secondly, the welded blank is tailored into a round blank by laser cutting. Ultimately, the hybrid manufacturing technique is utilized to gradually spin the TWB into the final TWCS, as shown in Fig. 1d.

Compared with the conventional combination manufacturing process of stamping and tailor welding, these components manufactured by FSW TWB spin-forming have a higher reliability and longer service life without fewer welding seams, and their microstructure and properties are also improved by the spinning processing.²⁸ In particular, metal scraps in many industries can also be re-utilized by adopting the hybrid manufacturing method based on spinning and FSW to minimize the waste of materials and resources, which is undoubtedly a green manufacturing method. Moreover, it is the most meaningful thing that the TWB spin-forming process contributes to an important approach to manufacturing large-diameter TWSCs.

EXPERIMENTAL MATERIAL AND PROCEDURES

Tailor-Welded Blank

In this study, TWBs were derived from commercial rolled and annealed 2195 Al-Li alloy blanks with the length and width of 400 × 400 mm and thickness of 3 mm, whose chemical composition is listed in Table 1. By FSW and laser-cutting, the TWBs were processed into 390-mm-diameter round blanks with a 10-mm-wide welding seam in their centerline. It is well known that the FSW process will produce different material properties from the BMZ. To analyze the deformation behaviors and characteristics during the TWBs spin forming, the material properties of the TWBs were divided into the BMZ and WZ. Combining with the method from the references,^{29,30} the microhardness measurement was conducted with a 0.5-mm spacing across the welding seam, while the base material and the measurements were set to 5 layers with a 0.5-mm spacing in the thickness direction of the welding seam. As a consequence, both horizontal profiles of Vickers hardness in the WZ and BMZ are described in Fig. 2.

To achieve the mechanical properties of the BMZ and WZ in the TWBs, the tensile specimen in the BMZ was cut from any BMZ, while the tensile specimen in the WZ was cut along the welding direction of the TWBs, and the width of the gauge section is the weld width obtained by the above microhardness measurement (Fig. 2). By tensile tests and calculations, the BMZ constitutive model was represented by the equation ($\sigma = 221.36 \times \varepsilon^{0.09}$), while the WZ constitutive model was represented by the equation ($\sigma = 252.63 \times \varepsilon^{0.11}$). The elastic modulus and yield strength of the base material are

79,000 MPa and 122.7 MPa, respectively, and those of the WZ are 73,000 MPa and 129 MPa, respectively.

Experimental Design and Equipment

The welding process parameters and spinning process parameters of the TWBs are listed in Table II. The FSW tool used in the double blanks welding consisted of a shoulder and a pin, with a shoulder diameter of 10 mm, and a 2.8-mm-long conical, grooved, threaded tri-flat pin. The FSW tool had an anticlockwise rotation with a 2.5° tilt and a plunge depth of 0.1 mm when welding was carried out. Figure 3 shows the spinning equipment and a schematic of the spinning mandrel. In the TWB spinning, double rollers were installed at a 45° angle to the spinning mandrel centerline, with the roller being 58 mm thick and 250 mm in diameter. The tailstock of 45 mm diameter was adopted to fix the TWB to the 45-mm-diameter surface of the spinning mandrel under hydraulic system thrust, as seen in Fig. 3a.

The TWB spin-forming process was developed by means of a spin machine (PS-CNCSXY1500HD) with double rollers. Single-pass shear spinning was used to form the TWSCs with the TWBs. Liquid drawing oil was used for lubrication, a mineral oil produced by Guangzhou Mechanical Engineering Research Institute, and applied to the surface of the spinning mandrel, rollers, and TWB, forming a dense lubricating film. Therefore, the liquid drawing oil has a small friction coefficient, good pressure resistance, and good adhesion to the metal surface

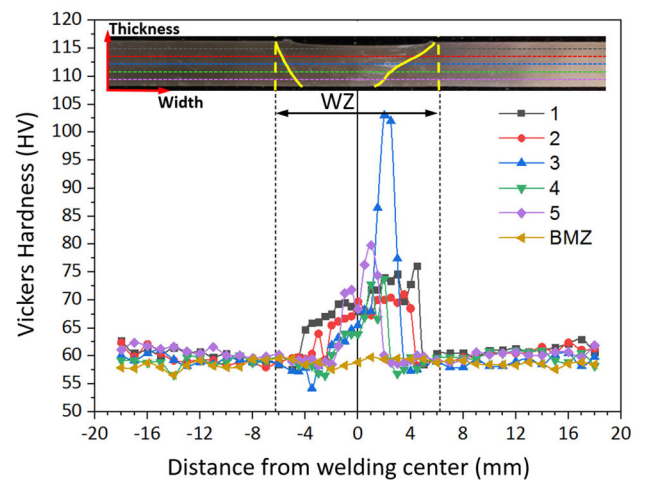


Fig. 2. Determination of WZ width by the microhardness distribution of 2195 Al-Li alloy FSW joint.

Table I. Chemical composition of 2195 Al-Li alloy (wt.%)

Element	Cu	Li	Mg	Ti	Zr	Fe	Si	Al
content	4.04	1.04	0.51	0.04	0.10	0.03	0.02	Bal

Table II. Welding and spinning process parameters of TWBs

Weld parameter	Value	Spinning parameter	Value
Welding feed speed (mm/min)	150	Roller operating angle (°)	45
Tool rotational speed (rpm)	800	Roller nose radius (mm)	10
Plunge depth (mm)	0.1	Mandrel rotational speed (rpm)	200
Shoulder diameter (mm)	10	Roller feed speed (mm/min)	400
Pin length (mm)	2.8	Spinning temperature (°)	25 °C
		Lubrication condition	Drawing oil

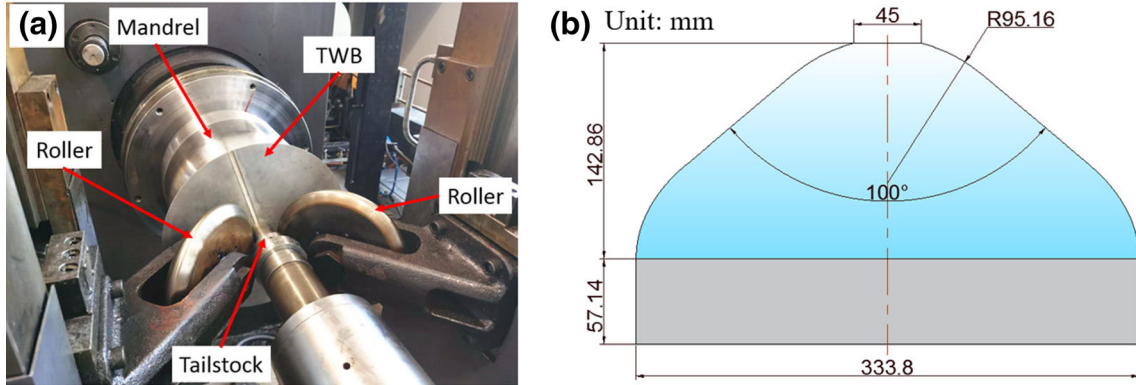


Fig. 3. Spinning set-up for thin-walled curved surface component: (a) spinning machine and (b) spinning mandrel.

during the TWB spin process. An INSTRON™ tensile tester was used to obtain the mechanical properties of the spun components, and a PX7™ ultrasonic thickness instrument with a measurement accuracy of 0.001 mm was used to obtain the wall thickness distribution of the spun components.

TWB Spinning Experiment

The TWB spin-forming experiment was performed under the parameters in Table II. The roller trajectory is strictly consistent with the sine law.³¹ The forming process of the spinning experiment for the TWCSs with FSW TWBs is shown in Fig. 4, and the final spun component was successfully obtained, as shown in Fig. 4g.

Finite Element Modeling

An FE model of TWBs shear spin forming was established based on ABAQUS/Explicit software to simulate the spinning deformation process of the TWCSs, as shown in Fig. 5a. In this model, the spinning mandrel was assumed to be a discrete rigid body, while the rollers were defined as analytical rigid bodies. The TWB with an original diameter of 390 mm and thickness of 3 mm was given to the deformable body. To simulate the TWB spinning deformation process of the material truly and efficiently, as shown in Fig. 5b, a three-dimensional (3D) 8-node reduced integration linear hexahedral element was adopted to mesh the TWB, and a 3D 4-node linear tetrahedral element was used as the

transition elements in the radial direction to adjust the aspect ratio of elements. Meanwhile, as shown in Fig. 5b, the elements in the second annular zone, in which the TWB will contact with the arc segment of the spinning mandrel during the TWBs spin forming, were densest so that the FE model can supply smooth contact between the spinning mandrel and TWB, and make the plastic bending deformation steadier. The number of elements in the thickness direction is two, which is sufficient to model the deformation in the thickness direction during the TWB spin-forming process.³² According to the microhardness measurement results of the material, as shown in Fig. 2, the WZ was separated from the TWB and the width of the WZ was determined to be 12.5 mm.

In the model, a coupling constraint was exerted on the fixed end of the blank to make the TWB and spinning mandrel rotate synchronously. The penalty friction equation and Coulomb's friction were adopted to represent the normal and sliding contact effect between the rollers and the TWB, respectively. The friction conditions were assigned as follows: the coefficient between the spinning mandrel and the TWB was 0.5, and the coefficient between the TWB and the rollers was 0.05.² In addition, the roller trajectory was calculated by the coordinate transformation relative to the reference point, which is strictly consistent with the sine law.

In order to determine the validity of the FE simulation model of the TWBs shear spin forming, the FE simulation results, including the flange

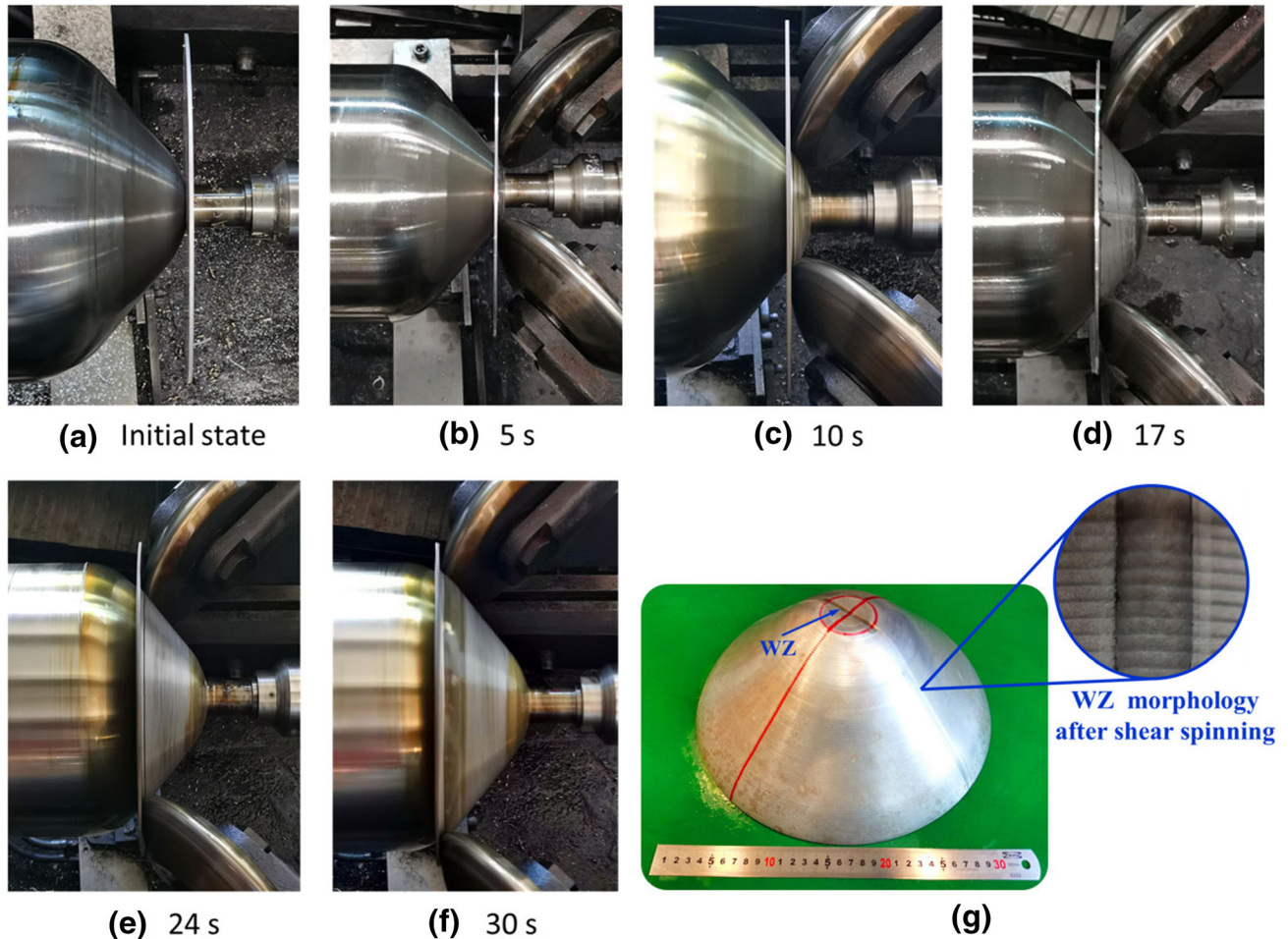


Fig. 4. Experiment results of TWBs shear spin forming.

(circumferential annular zone of the component that has not been spun) states (Fig. 5c), the wall thickness distributions (Fig. 6a, b), and the welding seam deflection angle in the FE simulation were compared to the shear spinning experiment results under the process conditions of Table II. The corresponding experimental results were generally consistent with the FE simulation results as shown in Fig. 6(c, h). Consequently, the developed FE simulation model of the TWB shear spin forming for the TWCS is reliable.

RESULTS AND DISCUSSION

Comparison of Deformation Characteristics Between TWBs and SIBs

Figure 7a, b shows the equivalent stress distributions of TWBs and SIBs shear spin forming under typical moments. It can be seen that the equivalent stress distribution feature of the TWBs is very similar to the SIBs at 10 s, while the equivalent stress distributions were obviously different at 17 s and 30 s. Specifically, for the SIBs spin forming, the equivalent stress located behind the roller contact zones roller was higher than in any other zones.

However, during the TWBs shear spin forming, it is only after 10 s that the equivalent stress located behind the contact zones of the roller was obviously high, as shown in Fig. 7a, b. Meanwhile, the equivalent stress in the WZ of the TWB spun component increased significantly at 30 s. In addition, it can be clearly seen from Fig. 7a, b that the equivalent stress distribution of the SIB spun component was more inhomogeneous than that of the TWBs spun component at 17 s and 30 s, which indicates that the material flow and deformation are sufficient during the SIB spinning.

In order to know the equivalent stress distribution laws of the TWBs shear spin forming, the maximum equivalent stresses of TWBs and SIBs shear spin-forming process under typical moments were analyzed, as shown in Fig. 7c. In different typical moments, the maximum equivalent stresses of deformation zones during the TWB shear spin forming were much higher than that of the SIBs shear spin forming. Apart from the 30 s, the maximum equivalent stresses showed a general uptrend which illustrated that the inhomogeneous deformation became more and more intense with the shear spin forming. According to Fig. 7, it can be

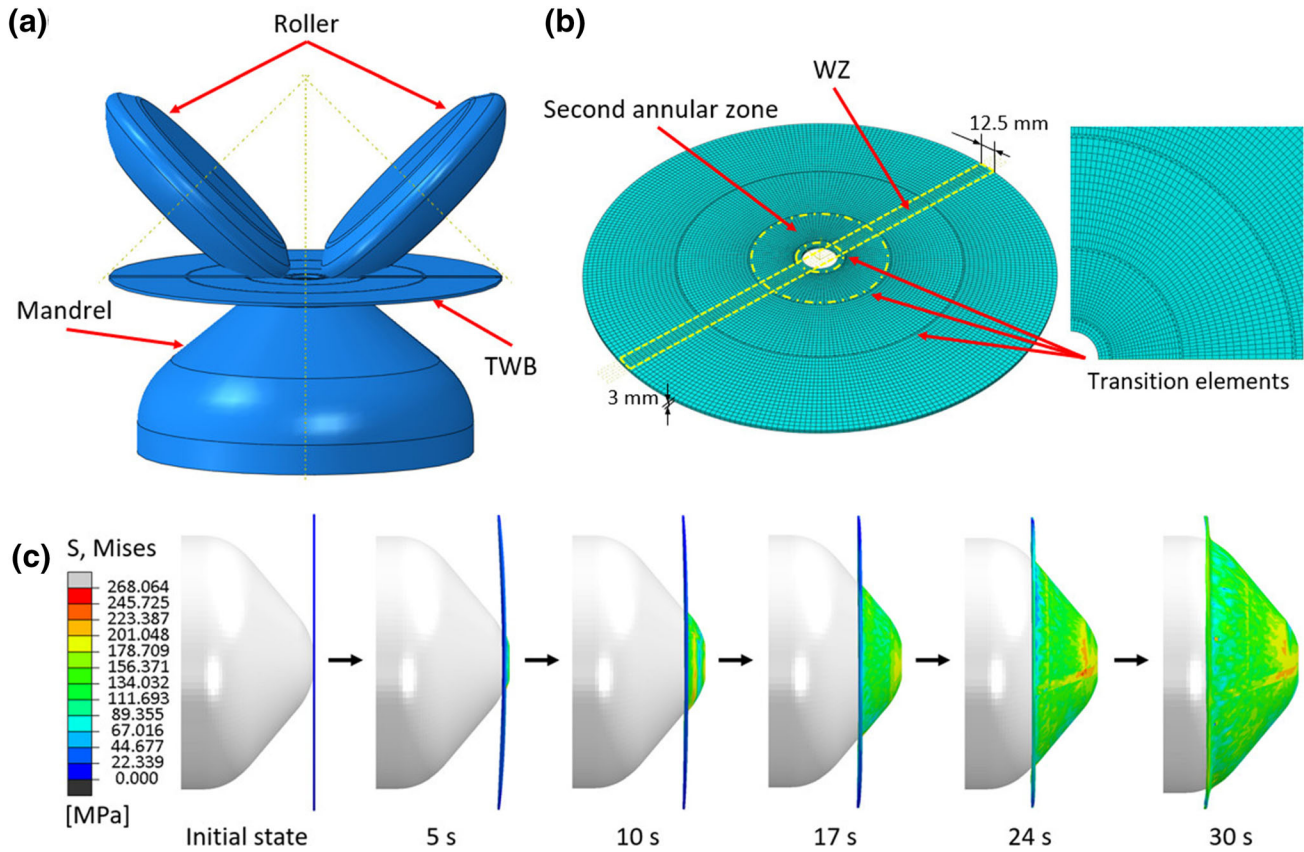


Fig. 5. Finite element model of TWBs shear spin forming: (a) geometry model, (b) meshing method, and (c) FE simulation results.

concluded that, although the maximum equivalent stresses of the SIB were smaller than those of the TWB, the equivalent stress distributions were more inhomogeneous. Therefore, the existence of a welding seam may restrict the material flow and plastic deformation during the TWB spin forming, which leads to the increase of the TWB equivalent stresses.

In addition, Fig. 4a–f shows the changes in the flange state during the TWBs shear-spinning experiment, from which it can be seen that the flange states are varying all the time with the spin forming. At 5 s, 10 s, and 17 s, the flange swing was more and more noticeable, and that the flange was inclined backward to the side of the rollers at 24 s, while the flange was inclined forward to the side of the machine spindle at 30 s. These laws are consistent with the results (Fig. 5c). As shown in Fig. 6c–f, with the TWB shear spinning, the equivalent stress distributions of TWBs were more and more inhomogeneous. It can be clearly seen that the equivalent stress distributions of the WZ of TWBs obviously increased at 21 s and 30 s, which indicated that the WZ contributes to the inhomogeneous plastic deformation and the flange swing.

Welding Seam Movement

There was an important and interesting observation: the welding seam of the spun component deviated from the original welding centerline of the TWBs in the experimental results of the TWBs shear spinning, namely, the deflection phenomenon of welding seam, as shown in Fig. 6c–h. It can be seen from this figure that the welding seam was straight before TWB shear spinning, while the welding seam of the TWBs spun component deflected after TWB spinning. According to the FE simulation results (Fig. 6c–f), as the plastic deformation increases, it can be found that the equivalent stress distributions of the WZ of TWBs were larger and larger, and at the end of the welding seam movement along the rotation direction of spun components. Finally, the deflection of the welding seam of the TWBs spun component occurred after spin forming. The deflection angle of the welding seam was also measured by a laser measuring instrument (Fig. 8a) to evaluate the deflection extent of the welding seam deviating from the welding centerline; the deflection angle was about $3^\circ \sim 4^\circ$, as shown in Fig. 6.

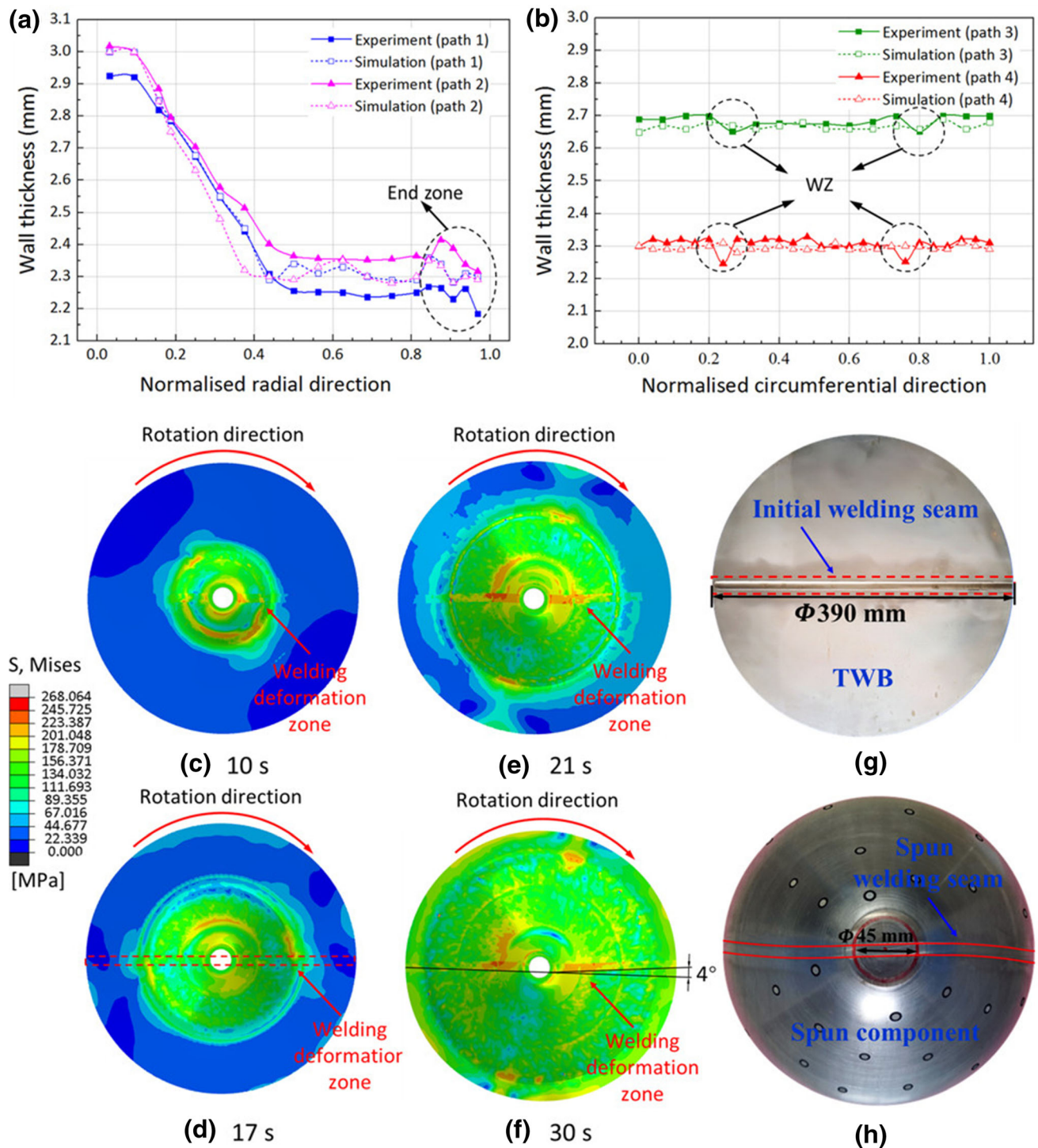


Fig. 6. Wall thickness distributions and welding seam movement of TWBs spun component: (a) radial paths: Path 1 (WZ) and Path 2, (b) circumferential paths: Path 3 and Path 4, (c–f) welding seam movement process in FE simulation, and (g, h) initial and spun welding seam.

Wall Thickness Distribution

The wall thickness is regarded as an important evaluation index for the forming quality in shear spinning. In this study, the wall thickness distributions along the radial and circumferential paths (Path 1, Path 2, Path 3, and Path 4) were analyzed, respectively, as shown in Fig. 8b. Path 1 is located

in the centerline of the WZ, while Path 2 is located in the BMZ and perpendicular to Path 1. And Path 3 and Path 4 are located in the arc and line segments of the spun component, respectively.

Figure 6a and b illustrates the wall thickness distributions of the TWB spun component along the typical radial and circumferential paths in the

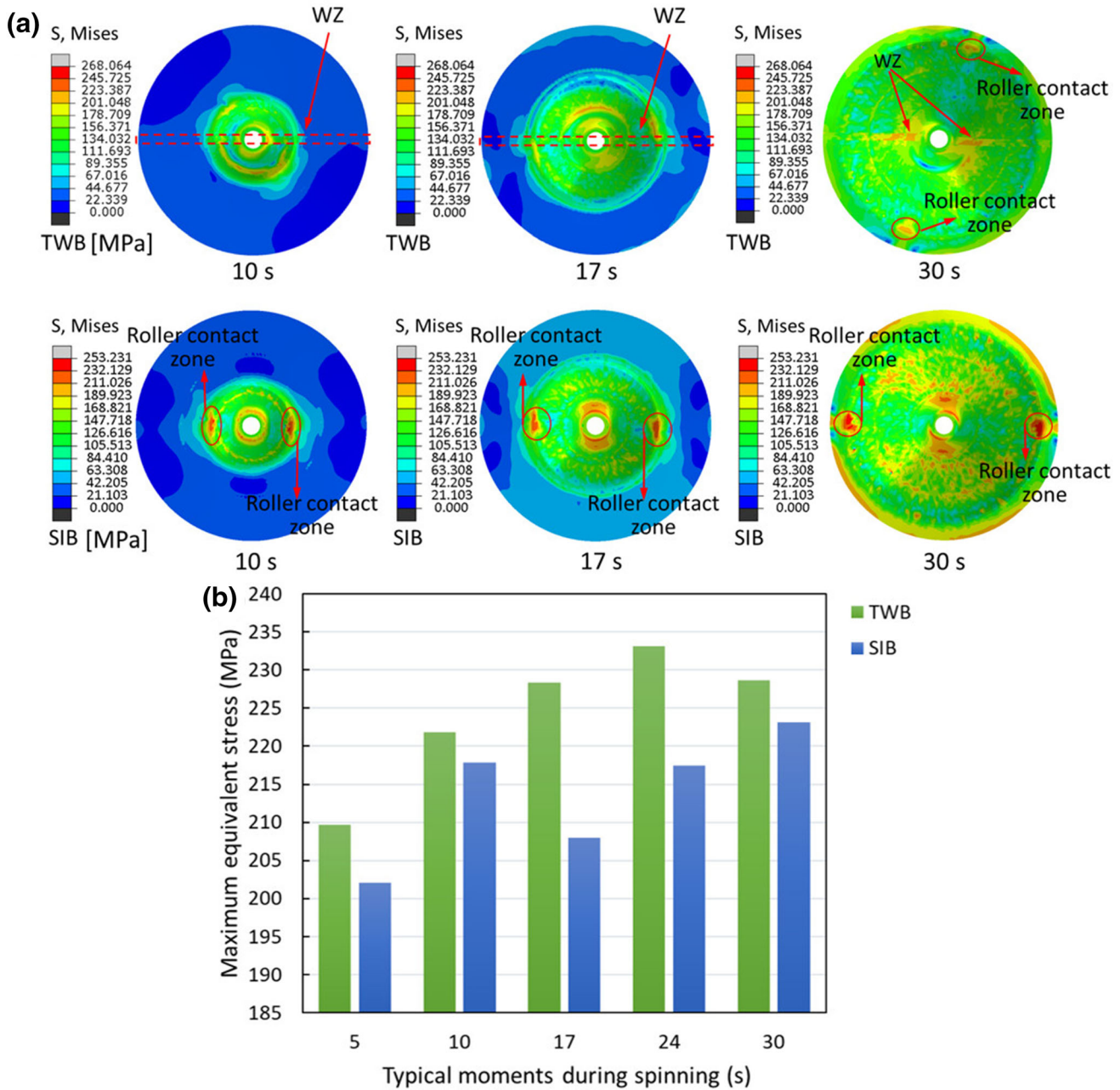


Fig. 7. Equivalent stress of TWB and SIB shear spinning under typical moments: (a) equivalent stress distributions and (b) maximum equivalent stresses.

spinning process. It can be observed from Fig. 6a that the wall thickness variation trend of Path 1 in the WZ is similar to Path 2. Moreover, the wall thickness values have a small fluctuation and obvious decrease in the end zone of the TWBs spun component, which was caused by the local thinning and inhomogeneous deformation with the half-cone angle of the spinning mandrel decreasing. As shown in Fig. 7, on the whole, during the TWB spinning, the equivalent stress of deformation zones gradually increases. Meanwhile, it can be found that the equivalent stress in the roller contact zone also increases. This suggests that equivalent stress

increase contributes to the fluctuation and the decrease of wall thickness in the end zone of the TWBs spun component. In addition, the wall thickness values of Path 1 were less than that of Path 2, which was mainly the reason of the wall thickness thinning caused by FSW in the WZ. Likewise, in Fig. 6b, the wall thickness values of Path 3 and Path 4 in the WZ were the smallest. However, compared with the original TWB, the wall thickness difference of the BMZ and WZ after TWBs spinning decreased. Therefore, the spinning process is beneficial in reducing the wall thickness inhomogeneity of the TWBs.

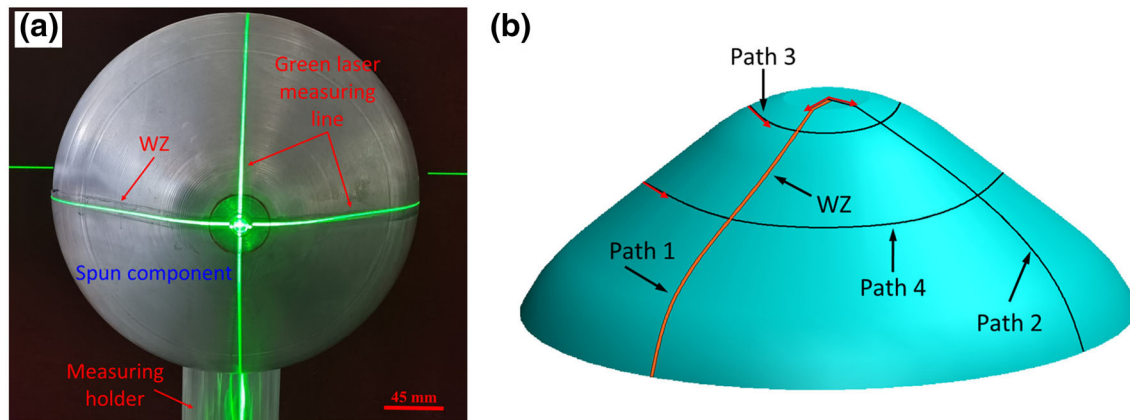


Fig. 8. (a) Measurement of the welding seam deflection angle and (b) schematic of the path selection for wall thickness analysis.

Microstructure and Properties

The microstructure and properties of the spun TWSCs with the 2195 Al-Li alloy TWBs produced by FSW have significant differences from the original material. After shear spin forming, in order to obtain the changes in material microstructure and properties, in this section, the microstructure, hardness, and mechanical properties have been analyzed.

Microstructure

As shown in Fig. 9, the microstructure was observed by electron back-scatter diffraction and the specimens were extracted along the normal direction (ND) and the transverse direction (TD) (similar to the circumferential direction of the spun component) from the spun component. The ND in all the sample coordinate systems is projected to the crystal coordinate system. Thus, the original and deformed microstructures in the WZ and BMZ were obtained. It can be seen in Fig. 9a that the original microstructure in the BMZ has a certain directivity and presents a larger fiber structure, which is the result of the sheet-rolling process. After the shear-spinning deformation, it is obviously seen in Fig. 9b that the directivity of the microstructure is more obvious and, compared with the original BMZ, the fiber structure is significantly refined. In addition, it can be observed from Fig. 9c, d that there are considerable differences in the microstructure between the original WZ and spun WZ. The microstructure of the original WZ was approximately equiaxed and had a uniform grain distribution, while the microstructure reflected an apparent directionality and fiber morphology after shear-spinning deformation. Meanwhile, according to the pole figures (PFs) (Fig. 9e–h), it can be observed from the PFs that, after spinning, strong crystal reorientations occurs in both the BMZ and WZ. The original texture of the BMZ and WZ is close to the $\langle 111 \rangle$ and $\langle 101 \rangle$ types, respectively, while both regions are orientated to

the $\langle 111 \rangle$ directions after spinning. The maximum intensity of the texture components are also increased after spinning. In addition, compared with the original microstructure, the grains of the BMZ and WZ gradually become thinner and longer. These factors contribute to the anisotropy of the spun component. The reason for this phenomenon is that continuous thinning and great shear deformation accumulation of material during shear spinning occurred.

Hardness

The hardness of the cross-sections in the original and spun WZ was measured by a digital microhardness tester. The test was carried out from the retreating side to the advancing side in the centerline of the cross-section of the WZ. Figure 10a displays the microhardness distribution curves of the WZ of the spun components. It can be seen that the microhardness distribution profiles in the original and spun WZ are similar, while the microhardness of the spun components in the WZ increased on average by 21% after spinning deformation. Zhang et al.³¹ have also found the phenomenon that microhardness obviously improves after the shear spinning process. Work hardening is mainly responsible for the elevated micro-hardness.

Mechanical Properties

The WZ is the vital part of the spun component with 2195 Al-Li alloy TWBs, which requires high strength. In this study, the mechanical properties of standard tensile specimens cut along the radial and circumferential directions from the BMZ and WZ (BMZ-R, BMZ-C, WZ-R, WZ-C) of the spun components were tested. Especially for the standard tensile specimens with the welding seams, the welding seams were required to be in the middle of the gauge section of standard tensile specimens. Figure 10b, c display the yield strength and tensile strength of standard tensile specimens with different zones, states, and directions. It can be observed

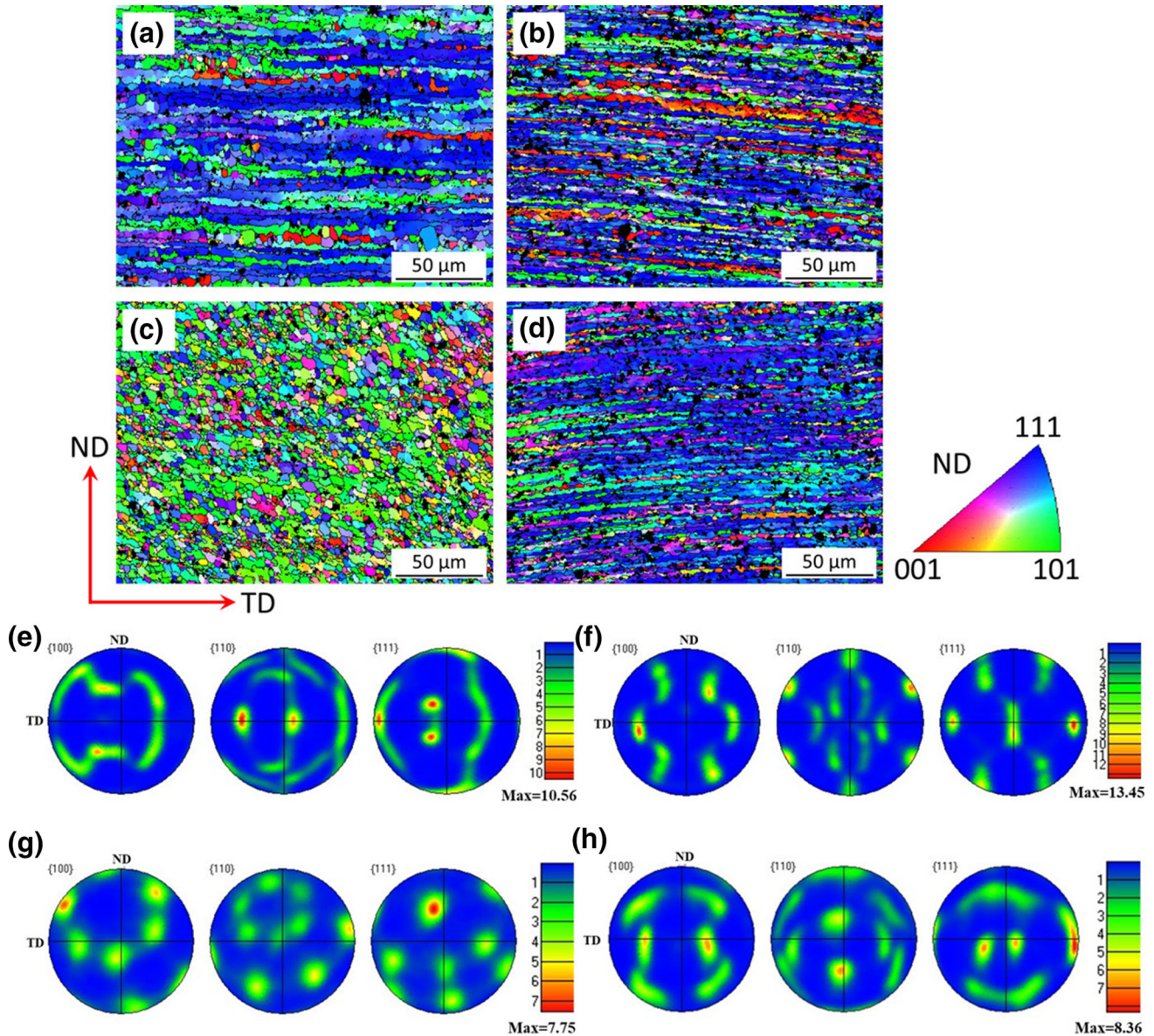


Fig. 9. Microstructure and PFs: (a, e) original BMZ, (b, f) BMZ after spinning, (c, g) original WZ and (d, h) WZ after spinning.

from Fig. 10b and c that the yield strength and tensile strength of spun components are all obviously higher than those of the original blanks. In particular, the yield strength of the materials increased most significantly after the shear-spinning process, as shown in Fig. 10b. Meanwhile, it can also be found that the increases of the tensile strength and yield strength in the WZ are all greater than those of the BMZ. As shown in Fig. 10b, after shear spinning, the yield strength of the BMZ-C and BMZ-R of the spun components are averagely increased by 38% and 46%, respectively, while the WZ-C and WZ-R of the spun components are significantly increased, on average, by 62% and 65%, respectively. In addition, it can be seen from Fig. 10c that the tensile strength of the BMZ-C and BMZ-R are increased, on average, by

9% and 7%, respectively, and the WZ-C and WZ-R of spun components are increased on average by 17% and 12%, respectively. It is also found that, after spinning, the elongation decreased significantly and the elongation of the WZ decreased by more than 60%. Zhan et al.³³ have also reported that significant work hardening and grain refinement will be produced under the shear spinning of aluminum alloys. Therefore, the mechanical properties of the TWBs can be significantly improved under the shear-spinning process.

CONCLUSIONS

A novel hybrid manufacturing technique combining friction stir welding and spinning was used to form 2195 Al-Li alloy thin-walled axisymmetric components. The deformation characteristics,

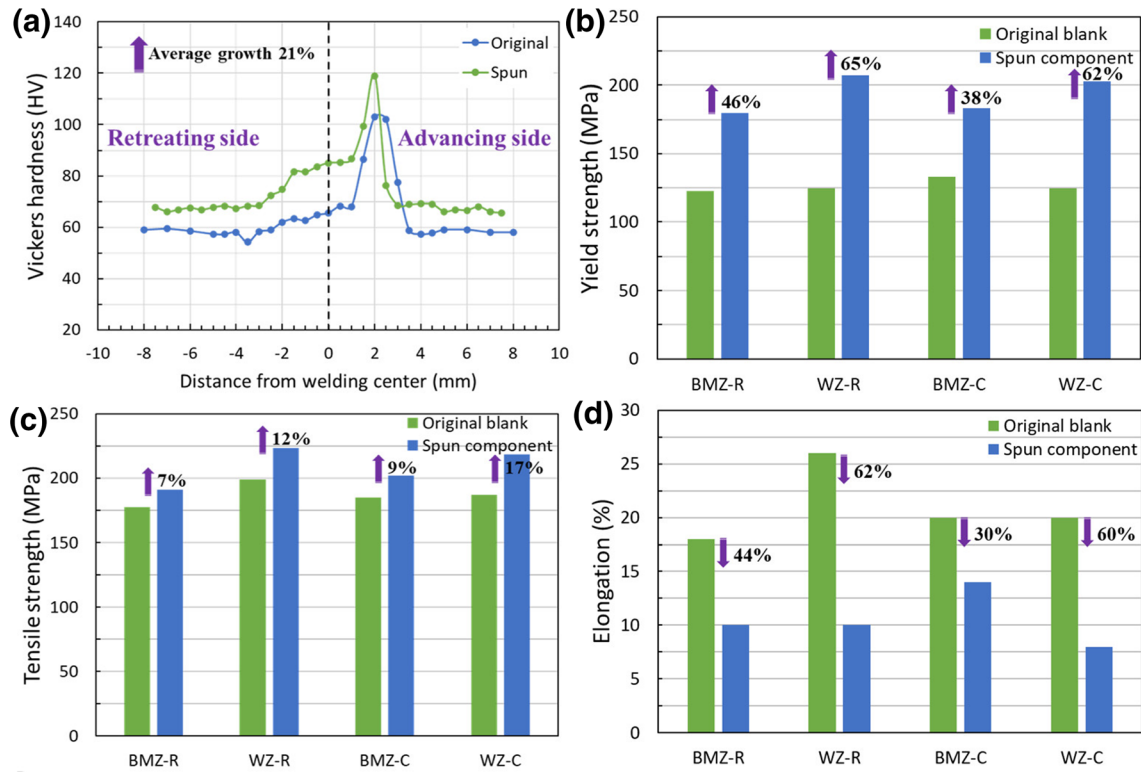


Fig. 10. (a) Hardness distribution of the WZ of the spun components, and (b) yield strength, (c) tensile strength, and (d) elongation of the spun components.

microstructure, and properties of the spun components were studied through spinning experiments together with finite element simulation on the TWBs spinning. The following conclusions can be drawn:

- (1) Because the welding seam of tailor welding blanks restricts the material flow and plastic deformation, the spinning deformation process of tailor-welded blanks is more inhomogeneous than that of single integrated blanks.
- (2) During spin forming of tailor-welded blanks, welding seam movement occurred with the rotating of the spun components. The deflection direction of the welding seam was consistent with the mandrel rotating direction. After spinning, the deflection angle of the welding seam was about $3^\circ \sim 4^\circ$. In addition, the spinning process is beneficial in reducing the wall thickness inhomogeneity caused by the welding thinning of FSW.
- (3) After spinning, compared with the properties of the original TWB, the microhardness of the spun components in the WZ is increased on average by 21%. The yield strength of the BMZ-C and BMZ-R of the spun components increased on average by 38% and 46%, respectively, while the WZ-C and WZ-R of spun components increased on average by 62% and 65%, respectively. In addition, the tensile strength of the BMZ-C and BMZ-R increased

on average by 9% and 7%, respectively, and the WZ-C and WZ-R of the spun components increased on average by 17% and 12%, respectively. The elongation decreased significantly and the elongation of the WZ decreased by more than 60%.

ACKNOWLEDGEMENTS

The authors acknowledge the funding support from the National Key R&D Program of China (Project 2020YFA0711100), the National Science Fund for Distinguished Young Scholars of China (Project 51625505), the National Natural Science Foundation of China (Project 52105399, Project U1937203 and Project U1910213) and the Natural Science Basic Research Plan in Shaanxi Province of China (Project 2020JQ-166).

CONFLICT OF INTEREST

The authors declare that they have no conflict of interest.

REFERENCES

1. A. Medjahed, B.C. Li, L.G. Hou, R.Z. Wu, A. Zegaoui, M. Derradji, and H. Benyamina, *JOM* 71, 4. (2019).
2. M. Zhan, J. Guo, M.W. Fu, P.F. Gao, H. Long, and F. Ma, *J. Mater. Process. Technol.* 257, 15. (2018).
3. E. Balducci, L. Ceschini, and S. Messieri, *JOM* 70, 11. (2018).

4. X.C. Meng, Y.X. Huang, J. Cao, J.J. Shen, and J.F. dos Santos, *Prog. Mater. Sci.* 115, 20. (2020).
5. Q.X. Xia, G.F. Xiao, H. Long, X.Q. Cheng, and X.F. Sheng, *Int. J. Mach. Tools. Manuf.* 85, 100. (2014).
6. X.S. Yang, W.J. Huang, X.H. Zhu, R. Zhang, F. Guo, and L. Hu, *Met. Mater. Int.* 27, 4793. (2021).
7. S. Chen, X.H. Zhan, Y.Q. Zhao, Y.F. Wu, and D.T. Liu, *Met. Mater. Int.* 27, 1671. (2021).
8. C.C. Wong, T.A. Dean, and J. Lin, *Int. J. Mach. Tools. Manuf.* 43, 1419. (2003).
9. D.Y. Yang, M. Bambach, J. Cao, J.R. Dufflou, P. Groche, T. Kuboki, A. Sterzing, A.E. Tekkaya, C.W. Lee, and C.I.R.P. Ann-Manuf, *Techn.* 67, 743. (2018).
10. P.F. Gao, C. Yu, M.W. Fu, L. Xing, and J. Guo, *Chinese. J. Aeronaut.* 35, 320. (2022).
11. B. Kinsey, Z.H. Liu, and J. Cao, *J. Mater. Process. Technol.* 99, 145. (2000).
12. M. Merklein, M. Johannes, M. Lechner, and A. Kuppert, *J. Mater. Process. Technol.* 214, 151. (2014).
13. J. Liu, A.L. Wang, H.X. Gao, J. Gandra, K. Beamish, L.H. Zhan, and L.L. Wang, *J. Mater. Process. Technol.* 257, 33. (2018).
14. M. Abbasi, S.R. Hamzeloo, M. Ketabchi, M.A. Shafaat, and B. Bagheri, *Int. J. Adv. Manuf. Tech.* 73, 999. (2014).
15. X.D. Ma, and Y.P. Guan, *Met. Soc. China* 26, 228. (2016).
16. M. Parente, R. Safdarian, A.D. Santos, A. Loureiro, P. Vilaca, and R.M.N. Jorge, *Int. J. Adv. Manuf. Tech.* 83, 2129. (2015).
17. M.H. Wang, J. Zhou, C.F. He, M. Yang, and F. Xiang, *J. Mech. Eng.* 45(245), 234. ((in Chinese)) (2009).
18. J.H. Zhang, Z.X. Chen, L.Q. Xu, and J.H. Yu, *Technology* 38, 156. ((in Chinese)) (2013).
19. Z.H. Yin, K. Liu, J.X. Yu, Y. Tian, and M.Z. Hu, *Technology* 41, 39. ((in Chinese)) (2016).
20. S.L. Ma, M.Z. Li, G. Sun, X.J. Li, and Z.R. Qian, *J. Jilin Univ. (Eng. Technol. Edition)*. 38, 334. ((in Chinese)) (2008).
21. Z. Zimniak, and A. Piela, *J. Mater. Process. Technol.* 106, 254. (2000).
22. X.G. Qiu and W.L. Chen, *J. Mater. Process. Technol.* 187, 128. (2007).
23. Y.P. Guan, L.J. Wang, A.S. Lv, J. Zhao, and L.X. Ma, *J. Plast. Eng.* 17, 28. ((in Chinese)) (2010).
24. X.J. Liu, W.H. Zhou, B. Liu, Z. Wang, and C. Wang, *Mater. Sci. Technol.* 23, 114. ((in Chinese)) (2015).
25. J.M. Wang, Y. Zhao, and Y.F. Jiang, *Forg. Stamp. Technol.* 32, 28. ((in Chinese)) (2007).
26. H.R. Zhang, M. Zhan, Z.B. Zheng, R. Li, W. Lyu, and Y.D. Lei, *Front. Mater.* 8, 1. (2021).
27. H.R. Zhang, M. Zhan, Z.B. Zheng, R. Li, F. Ma, X.L. Cui, S.W. Chen, and Y.D. Lei, *Int. J. Adv. Manuf. Tech.* 120, 3113. (2022).
28. G.F. Xiao, Q.X. Xia, and J.C. Long, *Int. J. Adv. Manuf. Tech.* 97, 2979. (2018).
29. T. Sakthivel, G.S. Sengar, and J. Mukhopadhyay, *Int. J. Adv. Manuf. Tech.* 43, 468. (2009).
30. Z. Yan, X. Liu, and H. Fang, *Int. J. Adv. Manuf. Tech.* 91, 3025. (2017).
31. J. Zhang, M. Zhan, H. Yang, Z.Q. Jiang, and D. Han, *Comp. Mater. Sci.* 53, 303. (2012).
32. K. Essa and P. Hartley, *Int. J. Mater. Form.* 2, 271. (2009).
33. M. Zhan, X.X. Wang, and H. Long, *Mater. Des.* 108, 207. (2016).

Publisher's Note Springer Nature remains neutral with regard to jurisdictional claims in published maps and institutional affiliations.